NISSUNA UMANA INVESTIGAZIONE SI PUO DIMANDARE VERA SCIENZIA
S'ESSA NON PASSA PER LE MATEMATICHE DIMOSTRAZIONI
LEONARDO DA VINCI

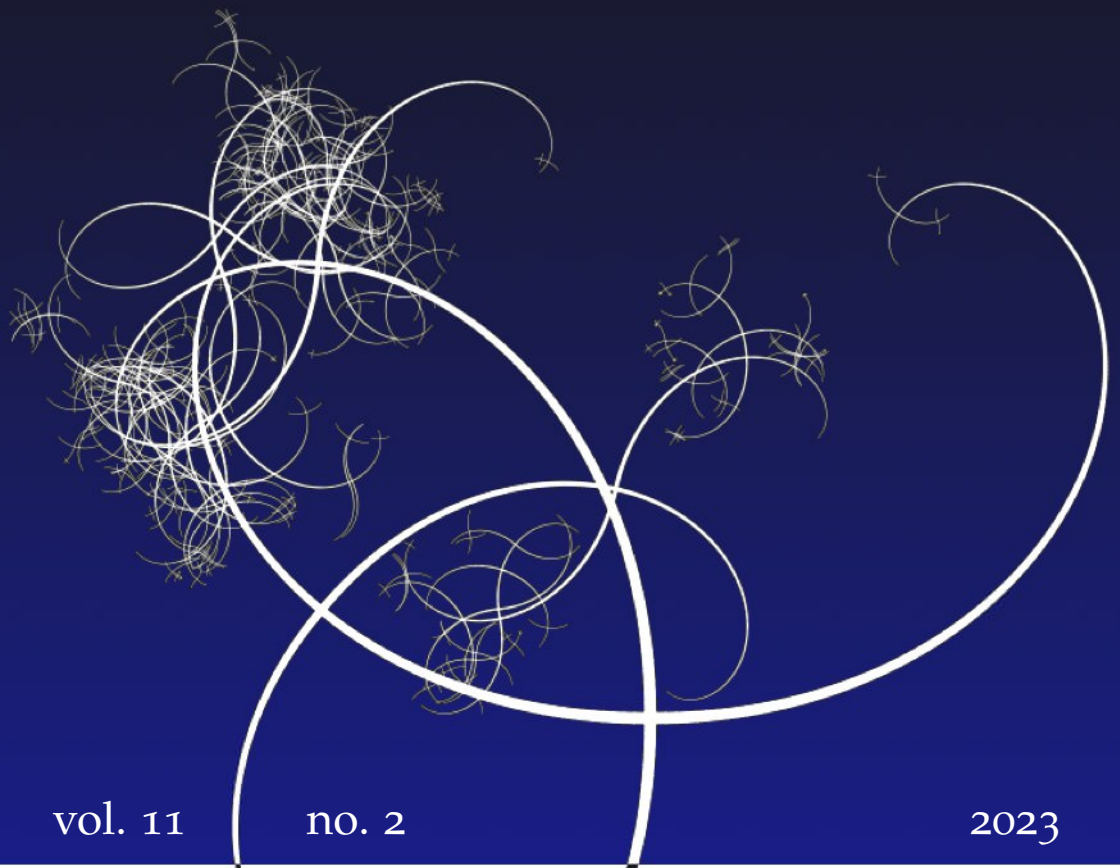

vol. 11 no. 2 2023

Mathematics and Mechanics *of* Complex Systems

Angelo Scrofani, Emilio Barchiesi,
Bernardino Chiaia, Anil Misra and Luca Placidi

FLUID DIFFUSION RELATED AGING EFFECT IN A CONCRETE DAM MODELED AS A TIMOSHENKO BEAM

msp

MATHEMATICS AND MECHANICS OF COMPLEX SYSTEMS
Vol. 11 (2023), No. 2, pp. 313–334
DOI: 10.2140/memocs.2023.11.313

FLUID DIFFUSION RELATED AGING EFFECT IN A CONCRETE DAM MODELED AS A TIMOSHENKO BEAM

ANGELO SCROFANI, EMILIO BARCHIESI, BERNARDINO CHIAIA, ANIL MISRA AND LUCA PLACIDI

Aging related damage within a concrete dam is often associated with the diffusion of certain particles which then activate internal chemical action. In this paper, a hemivariational method for a nonhomogeneous and damaged Timoshenko beam model is proposed in order to describe damage and deformation in a dam caused by the diffusion of an aging fluid.

The proposed model is used to perform a suite of parametric studies. In these studies, the dam is subjected not only to the concentrated and distributed external forces and couples (dual of displacement and rotation of the section, respectively) but also to the dual of the concentration of the aging fluid, called *external distributed aging fluid influx pressure*, that drives the incoming flow of the aging fluid which is, for this purpose, coupled with the damage evolution. The results are utilized to predict the life time of the dam. The life of big structures is a crucial point in civil engineering because it is linked with the safeguarding of human life.

1. Introduction

Dam health monitoring has been a continuous topic of interest for infrastructure maintenance [2; 7; 41; 68]. The life of concrete dams is affected by the diffusion of some deteriorating ions during its life time. The damage within a concrete dam is related to the distribution of such ions and it initiates when the concrete is subjected to tensile stress. As result, microcracks form and the damage begins to spread [28; 30; 60] because of the brittle behavior of the material [1; 46] and its low tensile strength. In this regard, it is worthwhile to note that the moisture content affects not only the mechanical response of a porous media, but it also activates the initiation of damage phenomena caused by creeping deformation, which during its transient phase induces a mechanical response (see [39; 65; 67]). This creeping deformation can cause sorption-induced aging phenomena [16]. Indeed,

Communicated by Francesco dell'Isola.
MSC2020: 74-XX.
Keywords: diffusion, dam, variational method, Karush–Kuhn–Tucker conditions, damage, aging.

the phenomenon of aging in the structures is a theme that finds application in various fields of engineering (e.g., [47]), in addition to civil engineering structures, and therefore, is a problem of wide interest. For the type of complex coupled diffusion-deformation-damage phenomena being considered in this work, the beam model [12; 24; 32; 43; 59] can serve as a feasible first step before considering the analysis of the more general 3-D problems. The beam theory has, in general, wide interest in the literature of deformable solid bodies (see, for example, [10; 13; 29; 31; 44]) as well as in the modeling of the aging phenomenon [8; 9; 42; 58]. Several studies have also focused on the chemical interactions between the dam material (concrete) and the aging elements, for example silicates (see [14; 15; 20; 21; 22; 23; 56]). Recently some works have focused also on the deformation dependency of the diffusion flux in solid [66] and polymeric gels or polymeric solids [40; 55]. In some formulations, e.g., [11], the damage evolution equation is assumed ab initio without a variational derivation or the consideration of the monolateral condition for the damage that is constrained to be a nondecreasing function of time.

In contrast, in [17] a hemivariational approach was considered for aging of concrete dams, in which one 3-D deformable body [6; 29] was modeled using a clamped Timoshenko beam model [4; 25; 26; 48; 64; 69]. However, the aging phenomenon was considered by decreasing arbitrarily a certain damage energy threshold. In particular a time dependent logarithmic law was used for describing the reduction of such a damage energy threshold. As a result the damage could increase with respect to time but it was not directly linked to the diffusion of deteriorating ions within the dam. Interrelationships between damage and these ions should be described by the use of proper coupling terms because of which the damage increases not only because of the external loads but also because of the presence of such a deteriorating fluid in the structure of the dam. Finally, a hemivariational approach is needed to model the irreversible and nondecreasing trend of the damage.

The aim of the present work is to use a variational approach [27; 33; 45; 49; 50; 51; 52; 54; 63], more specifically a hemivariational approach, in order to describe the aging phenomenon due to the spreading of aging fluid (for example, the salts) into the structure (concrete dam). The aging fluid can spread within the dam because imperfections are present in the concrete, such as through capillary phenomenon [5]. Following the approach first described in [17], a 1-D model is considered for the dam in this paper as well. The 3-D body is modeled as a 1-D Timoshenko beam which is subjected to several external loads due to (i) the pressure of the water, (ii) the self-weight of the dam and (iii) the *external distributed aging fluid influx pressure* that represents the dual of the fluid concentration. In this work, the damage threshold is linked with the concentration of the fluid by means of a proper damage-concentration coupling. During the analyzed dynamic

case, although the external loads do not change, displacements and deformations evolve as consequence of the reduction of the values of the stiffnesses due to the increasing values of the damage resulting from diffusion. The latter concept will be better discussed in Section 2.2 where the energy functional is presented. The dissipation phenomena during aging is taken into account by means of the Rayleigh functional, as in [19; 34], but other methods can be considered (e.g., in [18] where Dahl's modeled was used). As in [17], and also in this work, the concentration of the fluid is present within the energy functional. In addition parametric analyses are presented in order to explain the roles of the concentration-damage coupling and the diffusion coefficient. In conclusion, it is analyzed how the life of the dam changes when the previous parameters change.

2. Formulation of the nonhomogeneous Timoshenko beam problem with damage induced by age

2.1. ***Preliminary definitions.*** Body $\mathcal{B}$ is modeled as a 1-dimensional continuum [36; 37; 61] embedded in the 2-dimensional environment and its body points are characterized by means of the coordinate X in a given frame of reference. The set of kinematical descriptors, which depends upon the time t and the coordinate X, is composed of (i) the axial displacement $w = w(X, t)$, (ii) the transversal displacement $u = u(X, t)$, (iii) the rotation of the section $\vartheta = \vartheta(X, t)$, (iv) the concentration $c = c(X, t)$ of a fluid that is supposed to drive the damage evolution and (v) the damage field $\omega = \omega(X, t)$. The sign convention of the displacement components w and u and of the rotation ϑ are made explicit in Figure 1. Damage is an irreversible field whose value increases in time until the failure is reached. This phenomenon is represented by means of a scalar variable ω ranging from 0, denoting the undamaged case, to 1, denoting the complete failure.

2.2. ***Total deformation energy functional.*** Let $\mathcal{E}(w, u, \vartheta, c, \omega)$ be the *total deformation energy functional*, which depends upon all the kinematical descriptors listed

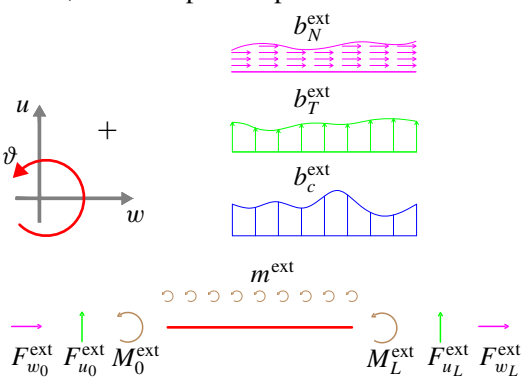

Figure 1. Signs convention.

previously. We note that the kinematical descriptors, as written in Section 2.1, are functions of the position X and the time t,

$$w(X,t), u(X,t), \vartheta(X,t), c(X,t), \omega(X,t) \quad \forall (X,t) \in [0,L] \times [t_0, +\infty), \tag{1}$$

where L is the length of the beam and t_0 is the initial time. The total deformation energy functional is assumed to have the form

$$\begin{aligned}
&\mathcal{E} = \mathcal{E}(w,u,\vartheta,c,\omega) \\
&= \int_0^L \left[\tfrac{1}{2}K_N(1-\omega)(w')^2 + \tfrac{1}{2}K_T(1-\omega)(u'-\vartheta)^2 + \tfrac{1}{2}K_M(1-\omega)(\vartheta')^2\right] dX \\
&\quad + \int_0^L \left[\tfrac{1}{2}K_{\mathrm{DIF}}(c')^2 + \tfrac{1}{2}K_F c^2 + K_{FN} c w' + K_{FT} c(u'-\vartheta) + K_{FM} c \vartheta'\right] dX \\
&\quad - \int_0^L [b_N^{\mathrm{ext}} w + b_T^{\mathrm{ext}} u + m^{\mathrm{ext}} \vartheta + b_c^{\mathrm{ext}} c]\, dX - F_{c0}^{\mathrm{ext}} c(0) - F_{cL}^{\mathrm{ext}} c(L) \\
&\quad - F_{w0}^{\mathrm{ext}} w(0) - F_{wL}^{\mathrm{ext}} w(L) - F_{u0}^{\mathrm{ext}} u(0) - F_{uL}^{\mathrm{ext}} u(L) - M_0^{\mathrm{ext}} \vartheta(0) - M_L^{\mathrm{ext}} \vartheta(L) \\
&\quad + \int_0^L \left[K_{\omega 0}\omega + K_{c\omega} c\omega + \tfrac{1}{2}K_\omega \omega^2\right] dX,
\end{aligned} \tag{2}$$

where K_N, K_T, K_M are the axial, shear and bending stiffnesses, respectively, b_N^{ext} is the distributed external axial load (dual of w), b_T^{ext} is the distributed external shear load (dual of u), m^{ext} is the distributed external couples (dual of ϑ), b_c^{ext} is the external distributed aging fluid influx pressure (dual of c), F_{c0}^{ext} and F_{cL}^{ext} represent the external concentrated fluid sources at $X=0$ and at $X=L$, respectively, F_{w0}^{ext} and F_{wL}^{ext} represent the external concentrated axial loads at $X=0$ and at $X=L$, respectively, F_{u0}^{ext} and F_{uL}^{ext} represent the external concentrated shear loads at $X=0$ and at $X=L$, respectively, and M_0^{ext} and M_L^{ext} represent the external concentrated couples at $X=0$ and at $X=L$, respectively (see Figure 1); also, K_{DIF} is a diffusion coefficient, K_F is the fluid elasticity, K_{FN} is the axial-fluid stiffness interaction, K_{FT} is the shear-fluid stiffness interaction and K_{FM} is the bending-fluid stiffness interaction. The terms $K_{\omega 0}$, $K_{c\omega}$ and K_ω represent the damage threshold, the concentration-damage coupling and the resistance to damage, respectively. It is worth noticing that the damage is defined by a real variable ω that is nondecreasing in time; so we assume the inequality

$$\frac{\partial \omega}{\partial t} \geq 0 \quad \forall X \in [0,L]. \tag{3}$$

The above condition implies the necessity of a generalization of standard variational principle into a so-called hemivariational principle. For simplicity let us define

$$\begin{aligned}
\Lambda &= (w,u,\vartheta,c,\omega), & \dot{\Lambda} &= (\dot{w},\dot{u},\dot{\vartheta},\dot{c},\dot{\omega}), \\
\delta\Lambda &= (\delta w,\delta u,\delta\vartheta,\delta c,\delta\omega), & \Delta\Lambda &= (\Delta w,\Delta u,\Delta\vartheta,\Delta c,\Delta\omega),
\end{aligned} \tag{4}$$

where Λ represents the set of the kinematical descriptors and $\dot{\Lambda}$, $\delta\Lambda$ and $\Delta\Lambda$ represent, respectively, the derivative with respect the time, the first variation and the increment of the Λ elements. It follows, trivially,

$$\Lambda + \delta\Lambda = (w + \delta w, u + \delta u, \vartheta + \delta\vartheta, c + \delta c, \omega + \delta\omega), \tag{5}$$

$$\Lambda + \Delta\Lambda = (w + \Delta w, u + \Delta u, \vartheta + \Delta\vartheta, c + \Delta c, \omega + \Delta\omega). \tag{6}$$

The subscript ω indicates the set

$$\Lambda_\omega = \Lambda - \{\omega\} = \{w, u, \vartheta, c\} \tag{7}$$

2.3. ***Hemivariational inequality principle.*** As in [54], a monotonically increasing time sequence $T_i \in \{T_i\}_{i=0}^n$ with $T_i \in \mathbb{R}_0^+$ and $n \in \mathbb{N}$ is introduced, including an initial and trivial datum (at $t_0 = T_0$) for each of the fundamental kinematical quantities. Let us consider the set of kinematically admissible placements and the kinematically admissible variations of the placements. Also note that the admissible variation of the irreversible kinematic quantity ω must be positive, and hence

$$\delta\omega \in \mathbb{R}_0^+. \tag{8}$$

Now, the first variation of the energy functional is calculated as follows:

$$\delta\mathcal{E}(\Lambda, \delta\Lambda) = \mathcal{E}(\Lambda + \delta\Lambda) - \mathcal{E}(\Lambda), \tag{9}$$

where the terms of order 2 or higher can be neglected. Let us consider that, at the i-th instant T_i, the increment of the fundamental kinematic quantities is calculated by the difference between these quantities as evaluated at the times T_i and T_{i-1}, namely,

$$\Delta\Lambda = (\Lambda)_{T_i} - (\Lambda)_{T_{i-1}}, \tag{10}$$

and the increment of the energy functional has the consequent definition

$$\Delta\mathcal{E}(\Lambda, \Delta\Lambda) = \mathcal{E}(\Lambda + \Delta\Lambda) - \mathcal{E}(\Lambda). \tag{11}$$

As in (9) the terms of order 2 or higher can be neglected. The Rayleigh functional is a quadratic form of the velocity-fields,

$$\mathcal{R}(\dot{\Lambda}_\omega) = \int_0^L \left[\tfrac{1}{2}c_w\dot{w}^2 + \tfrac{1}{2}c_u\dot{u}^2 + \tfrac{1}{2}c_\vartheta\dot{\vartheta}^2 + \tfrac{1}{2}c_c\dot{c}^2\right] dX \tag{12}$$

and its variation and increment, respectively, are defined as follows:

$$\delta\mathcal{R}(\dot{\Lambda}_\omega, \delta\Lambda_\omega) = \int_0^L [c_w\dot{w}\delta w + c_u\dot{u}\delta u + c_\vartheta\dot{\vartheta}\delta\vartheta + c_c\dot{c}\delta c]\, dX, \tag{13}$$

$$\Delta\mathcal{R}(\dot{\Lambda}_\omega, \Delta\Lambda_\omega) = \int_0^L [c_w\dot{w}\Delta w + c_u\dot{u}\Delta u + c_\vartheta\dot{\vartheta}\Delta\vartheta + c_c\dot{c}\Delta c]\, dX. \tag{14}$$

In order to get governing equations for this newly introduced model, we assume that the motion $w(X,t)$, $u(X,t)$, $\vartheta(X,t)$, $c(X,t)$ and $\omega(X,t)$ satisfies the hemi-variational principle

$$\Delta\mathcal{E}(\Lambda,\Delta\Lambda)+\Delta\mathcal{R}(\dot{\Lambda}_\omega,\Delta\Lambda_\omega)\leq\delta\mathcal{E}(\Lambda,\delta\Lambda)+\delta\mathcal{R}(\dot{\Lambda}_\omega,\delta\Lambda_\omega) \tag{15}$$

for any admissible variation $\delta\Lambda$, $\delta\Lambda_\omega$ of the fundamental kinematic quantities. The variational principle implies Euler–Lagrange equations of different types:

(i) a system of partial differential equations for a nonhomogeneous Timoshenko beam with the reduced stiffnesses due to damage and with a modified stress free reference configuration due to the fluid concentration ($K_{FN}c$ modifies the axial force, $K_{FT}c$ modifies the shear force and $K_{FM}c$ modifies the bending moment):

$$N'+b_N^{\text{ext}}=c_w\dot{w}, \tag{16}$$
$$V'+b_T^{\text{ext}}=c_u\dot{u}, \tag{17}$$
$$V+M_b'+m^{\text{ext}}=c_\vartheta\dot{\vartheta}, \tag{18}$$

with the definitions

$$N=K_N(1-\omega)w'+K_{FN}c, \tag{19}$$
$$V=K_T(1-\omega)(u'-\vartheta)+K_{FT}c, \tag{20}$$
$$M_b=K_M(1-\omega)\vartheta'+K_{FM}c, \tag{21}$$

and where N, V, and M_b represent the normal force, the shear force and the bending moment, respectively;

(ii) a differential equation for the diffusion of the fluid that is characterized not only by the external distributed aging fluid influx pressure b_c^{ext} but also by deformations (by the axial deformation $K_{FN}w'$, by the shear deformation $K_{FT}(u'-\vartheta)$ and by the bending deformation $K_{FM}\vartheta'$), by the concentration itself K_Fc and by damage $K_{c\omega}\omega$:

$$[K_{\text{DIF}}c']'+b_c^{\text{ext}}=c_c\dot{c}+K_{FN}w'+K_{FT}(u'-\vartheta)+K_{FM}\vartheta'+K_Fc+K_{c\omega}\omega; \tag{22}$$

(iii) a proper set of boundary conditions that yield

$$[N-F_{wL}^{\text{ext}}]\delta w=0,\quad X=L, \tag{23}$$
$$[N+F_{w0}^{\text{ext}}]\delta w=0,\quad X=0, \tag{24}$$
$$[V-F_{uL}^{\text{ext}}]\delta u=0,\quad X=L, \tag{25}$$
$$[V+F_{u0}^{\text{ext}}]\delta u=0,\quad X=0, \tag{26}$$
$$[M_b-M_L^{\text{ext}}]\delta\vartheta=0,\quad X=L, \tag{27}$$
$$[M_b+M_0^{\text{ext}}]\delta\vartheta=0,\quad X=0, \tag{28}$$
$$[K_{\text{DIF}}c'-F_{cL}^{\text{ext}}]\delta c=0,\quad X=L, \tag{29}$$
$$[K_{\text{DIF}}c'+F_{c0}^{\text{ext}}]\delta c=0,\quad X=0; \tag{30}$$

(iv) and a Karush–Kuhn–Tucker (KKT) condition

$$[\omega - \omega_T]\Delta\omega = 0, \quad \forall X \in [0, L], \tag{31}$$

where

$$\omega_T(X,t) = \left[\frac{1}{2}\frac{K_N}{K_\omega}(w')^2 + \frac{1}{2}\frac{K_T}{K_\omega}(u' - \vartheta)^2 + \frac{1}{2}\frac{K_M}{K_\omega}(\vartheta')^2\right] - \left[\frac{K_{\omega 0}}{K_\omega} + \frac{c \cdot K_{c\omega}}{K_\omega}\right]. \tag{32}$$

From this KKT condition and from the initial undamaged condition $\omega(X,0) = 0$, the damage variable ω starts to increase when the *normalized undamaged strain energy*

$$\frac{1}{2}\frac{K_N}{K_\omega}(w')^2 + \frac{1}{2}\frac{K_T}{K_\omega}(u' - \vartheta)^2 + \frac{1}{2}\frac{K_M}{K_\omega}(\vartheta')^2 \tag{33}$$

reaches the *normalized undamaged energy threshold*

$$\frac{K_{\omega 0}}{K_\omega} + \frac{c \cdot K_{c\omega}}{K_\omega}. \tag{34}$$

For the fluid to have an aging effect, we require the restriction on the coupling term

$$K_{c\omega} < 0. \tag{35}$$

Note that from (32) this restriction will result in the reduction of the energy threshold. Further thermodynamic restrictions are due to the needed positive definiteness of the strain energy. It is worth noting that, among such conditions, we also have

$$K_{c\omega}^2 < K_\omega K_F. \tag{36}$$

3. Beam representation of dam

The dam is usually conceived to have a trapezoidal shape, in a 2-D model, and clamped at the bottom. It is, therefore, modeled here by means of a *cantilever beam* as shown in Figure 2 in which the external and triangular distributed loads are considered due to both the water pressure and the self-weight. According to the model presented in [17] and the geometry that is shown in Figure 2, the water is on the left-hand side and the air is on the right-hand side. As shown in Figure 2, the red line (the geometric locus of the middle points of the sections) represents the 1-D beam by means of which the dam is modeled. In Figure 2, β and β' are the angles between the vertical line and, respectively, the 1-D beam and the left-hand side oblique surface of the dam. Thus, passing to the 1-D model, the weight of the dam must be considered on the mean line (the red line) as a triangular distributed external load (with both normal and orthogonal components) while the pressure of the water, because it is applied to the oblique surface of the dam, must be considered not only as a triangular distributed external load (with both normal and orthogonal components) but also as a triangular distributed external couple.

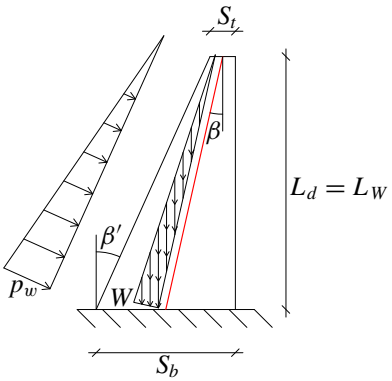

Figure 2. Dam profile.

Because the concentration of the fluid is affected by its pressure, it is reasonable to think that the distribution of the external distributed aging fluid influx is higher at the bottom of the dam. In the considered model the water height L_w is equal to that of the dam L_d. Hence, in the 1-D model a triangular distribution of b_c^{ext} is considered which has the higher value at the clamped end (for $X = 0$) and zero value at the top (for $X = L/\cos\beta$) as it will be shown in (40). The water pressure is due to Stevino's law; it is directed orthogonal to the left-hand side of the trapezoidal shape and the maximum value is p_w. The self-weight is directed vertically and the maximum value is W: in formulas,

$$p_w = \gamma_w g L_w \quad \text{and} \quad W = \gamma_c g L_d, \tag{37}$$

where γ_w and γ_c represent the mass density of the water and of the concrete, respectively. Notice that the weight of the dam is a distributed load on the domain while the pressure of the water is on the upstream facet (on the left-hand side of the trapezoidal shape) of the dam.

3.1. ***Stiffnesses identification.*** The stiffness of a given material is defined both by the Lamé coefficients λ and μ or by Young's modulus E and Poisson's ratio ν. First of all, we recall their relations,

$$\lambda = \frac{E \cdot \nu}{(1+\nu)(1-2\nu)}, \quad \mu = \frac{E}{2(1+\nu)}. \tag{38}$$

Thus, it is possible, as in [57], to identify the axial, shear and bending stiffnesses K_N, K_T and K_M as follows:

$$\begin{aligned} K_N(X) &= \frac{4\mu(\lambda+\mu)}{\lambda+2\mu} s(X) \cdot t_h, \\ K_T(X) &= \tfrac{2}{3}\mu \cdot s(X) \cdot t_h, \\ K_M(X) &= \frac{4\mu(\lambda+\mu)}{\lambda+2\mu} \frac{[s(X)]^3}{12} \cdot t_h, \end{aligned} \tag{39}$$

where t_h is the depth, i.e., the out-of-plane dimension of Figure 2 of the dam and where a rectangular cross-section is considered.

3.2. ***The distributed external loads.*** By assuming that b_c^{ext} is proportional to the pressure of the water and, therefore, it has a triangular distribution

$$b_c^{\text{ext}}(X) = b_{c,\max}^{\text{ext}}\left(1 - \frac{X}{L_w}\right) \cdot H(L_w - X \cdot \cos\tilde{\beta}), \tag{40}$$

and following the considerations about the weight of the dam and the pressure of the water at the beginning of the Section 3, the distributed external loads must be decomposed along the parallel and transverse directions of the beam as in [17]:

$$b_N^{\text{ext}}(X) = -t_h\gamma_w \sin(\tilde{\beta}'-\tilde{\beta})(L_w - X\cdot\cos\tilde{\beta})\cdot H(L_w - X\cdot\cos\tilde{\beta}) - \gamma_c t_h s(X)\cos\tilde{\beta}, \tag{41}$$

$$b_T^{\text{ext}}(X) = -t_h\gamma_w \sin(\tilde{\beta}'+\tilde{\beta})(L_w - X\cdot\cos\tilde{\beta})\cdot H(L_w - X\cdot\cos\tilde{\beta}) - \gamma_c t_h s(X)\sin\tilde{\beta}, \tag{42}$$

and the external distributed couple is

$$m^{\text{ext}}(X) = \tfrac{1}{2} t_h s(X)\gamma_w (L_w - X\cdot\cos\tilde{\beta})\cdot H(L_w - X\cdot\cos\tilde{\beta}), \tag{43}$$

where (i) X is the abscissa of the beam, (ii) L_w is the height of the water, (iii) s_t and s_b, represented in Figure 2, are the thickness at the top and at the bottom section of the dam, respectively, (iv) γ_c and γ_w are the density of the materials (as shown in the (37)), and (v) the subscripts c and w refer to concrete and water, respectively. Finally, the function $H(\zeta)$ is the Heaviside function to set to zero the contribution of water pressure above its maximum elevation, that is,

$$H(\zeta) = \begin{cases} 1, & \zeta \geq 0, \\ 0, & \zeta < 0. \end{cases} \tag{44}$$

4. Numerical investigation

The developed model is applied to perform parametric analyses by varying the values of K_{DIF} and $K_{c\omega}$ and for different spatial distributions of b_c^{ext}.

4.1. ***Uncoupled concentration c and the kinematic descriptors w, u, ϑ case.*** We note that concrete dam deformations (w', $u' - \vartheta$ and ϑ'), from (19), (20) and (21), are not expected to be affected by the density of the aging fluid. In the presented analyses, all the coupling terms K_{FN}, K_{FT}, K_{FM} are considered negligible:

$$K_{FN} = 0\,\frac{\text{J}}{\text{kg}}, \quad K_{FT} = 0\,\frac{\text{J}}{\text{kg}}, \quad K_{FM} = 0\,\frac{\text{m}^3}{\text{s}^2}. \tag{45}$$

In this case, the dam does not have a sponge-like behavior, which could be of interest for many other porous materials. The considered structural model and loading is shown in Figure 3 and the adopted parameters are reported in Table 1, where L_d is the height of the dam and L is the length of the equivalent beam. The

$L_d = L_w = 10\,\text{m}$	$b^{\text{ext}}_{c,\max} = 5 \cdot 10^5\ \frac{\text{J}}{\text{kg}}$
$s_t = 1\,\text{m}$	$K_{\text{DIF}} = 10^5\ \frac{\text{m}^5}{\text{kg}\cdot\text{s}^2}$
$s_b = 3\,\text{m}$	$K_F = 10^7\ \frac{\text{m}^3}{\text{kg}\cdot\text{s}^2}$
$\tilde{\beta} = \arctan\frac{s_b - s_t}{2L} = 0.1\,\text{rad}$	$c_c = 10^{16}\ \frac{\text{m}^3}{\text{kg}}$
$\tilde{\beta}' = \arctan\frac{s_b - s_t}{L} = 0.2\,\text{rad}$	$K_{c\omega} = -9 \cdot 10^5\ \frac{\text{J}}{\text{kg}}$
$L = \frac{L_d}{\cos\tilde{\beta}} = 10.05\,\text{m}$	$K_{\omega 0} = 800\,\text{N}$
$E = 4 \cdot 10^4\,\text{MPa}$	$K_\omega = 10^5\text{N}$
$t_h = 1\,\text{m}$	$\gamma_w = 10\ \frac{\text{kN}}{\text{m}^3}$
$\nu = 0.2$	$\gamma_c = 24\ \frac{\text{kN}}{\text{m}^3}$
$\lambda = 1.1 \cdot 10^{10}\,\text{MPa}$	$t_f = 3 \cdot 10^9\,\text{s} \approx 95\,\text{years}$
$\mu = 1.67 \cdot 10^{10}\,\text{MPa}$	

Table 1. Parameters for numerical investigation

values of the parameters are chosen according to [17]. However, two parametric analyses have been performed for the values of the new parameters K_{DIF} and $K_{c\omega}$. The results are shown in Sections 4.3 and 4.4. All the analyses have been carried out using the FEM software Comsol considering the (i) kinematic boundary conditions

$$w(0,t) = 0, \quad u(0,t) = 0, \quad \vartheta(0,t) = 0 \tag{46}$$

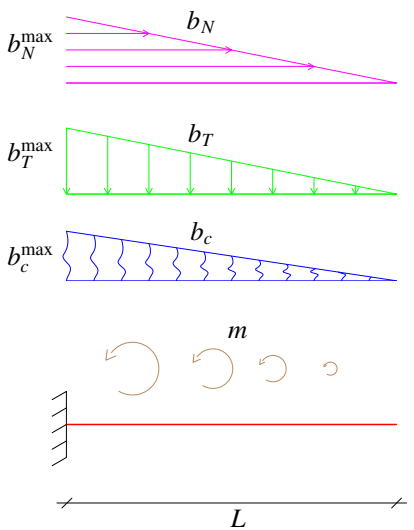

Figure 3. Cantilever beam model.

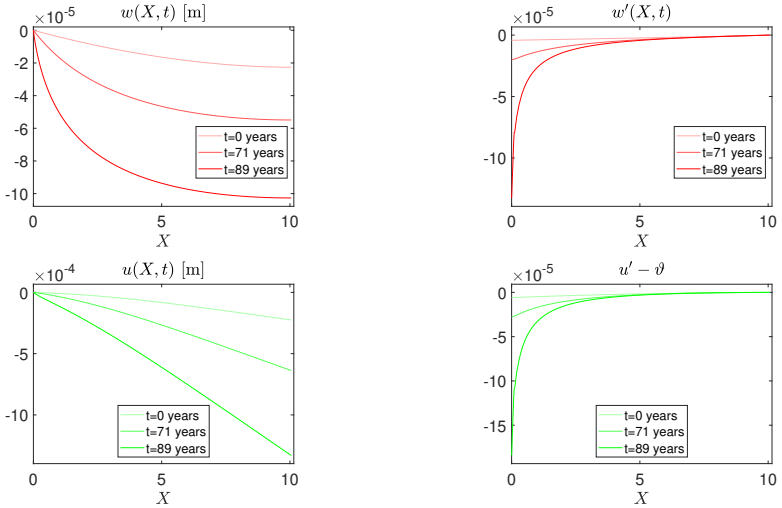

Figure 4. Top left: axial displacement $w(X,t)$. Top right: strain $w'(X,t)$. Bottom left: transversal displacement $u(X,t)$. Bottom right: shear deformation $u' - \vartheta$. The evolution in time of the kinematic quantities by a color gradient is represented. The aging evolution is represented from the lightest color to the most defined one.

and (ii) initial values

$$w(X,0) = 0, \quad u(X,0) = 0, \quad \vartheta(X,0) = 0. \tag{47}$$

The value of the damage threshold ω_T, for each time step, is prescribed in (32). The value of damage ω at a given time is taken to be the maximum between ω_T and the value of ω at the previous time step to update step-by-step according the KKT condition (32). It is noted that the KKT condition imposes the constraint that the damage always increases in time, so that the monolateral condition for the damage ω is met.

Figures 4 and 5 give the results of this analysis. It is worth noting that the kinematical descriptors w, u and ϑ evolve in time not because of the increase in the external loads, but because of the increase of damage ω, which results in the reduced values of the stiffnesses K_N, K_T and K_M in (19), (20) and (21). The negative values of w for $X > 0$ shown in Figure 4, top left, are reasonable because of the considered external gravity load. This results in the loss of strength of the dam.

Thus, the axial deformation w' is, as shown in Figure 4, top right, negative near the base (at $X = 0$) and null at the free side at $X = L$. The modulus of both the axial displacement and deformation are increasing functions of time. Similar observations are made for the transverse displacement from Figure 4, bottom left,

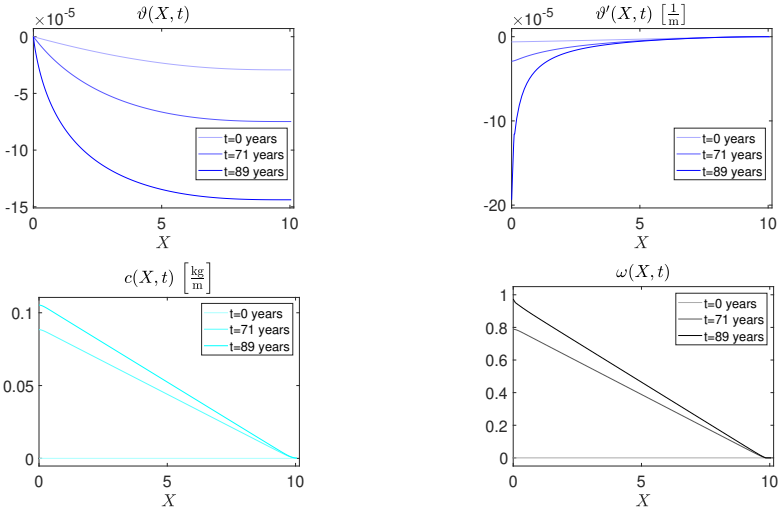

Figure 5. Top left: rotation of the sections $\vartheta(X,t)$. Top right: curvature ϑ'. Bottom left: concentration $c(X,t)$. Bottom right: damage $\omega(X,t)$. The evolution in time of the kinematic quantities by a color gradient is represented. The aging evolution is represented from the lightest color to the most defined one.

and the shear deformation in Figure 4, bottom right, and for the rotation in Figure 5, top left, and the curvature in Figure 5, top right.

The concentration of the aging fluid and the damage are shown in Figure 5, bottom left and bottom right, respectively. It can be seen that the aging fluid concentration and the damage, because they are coupled by the term $K_{c\omega}$, are both higher at the bottom of the beam at $X = 0$. So, if one increases, the other one increases as well. Finally, it is worth noting that, once damage reaches the unity value (at $X = 0$), the collapse of the dam is expected.

4.2. ***Parametric analysis: distribution of*** b_c^{ext}**.** We evaluate the behavior of the beam subjected to different b_c^{ext} distributions. The real distribution of b_c^{ext} is not known without measurements. Thus, we consider different distributions for demonstrating the potential effects. In order to compare the results with the triangular case, the integral of b_c^{ext} on the domain remains the same as that of the previous triangular case. Here, as an example, the externally distributed aging fluid influx pressure has been considered having a half gaussian curve distribution (see Figure 6). The half gaussian curve has the peak at $X = 0$. The parameters of the half gaussian distribution is such that

$$\int_0^L b_{c,\mathrm{triangular}}^{\mathrm{ext}}\, dX = \int_0^L b_{c,\mathrm{gaussian}}^{\mathrm{ext}}\, dX. \tag{48}$$

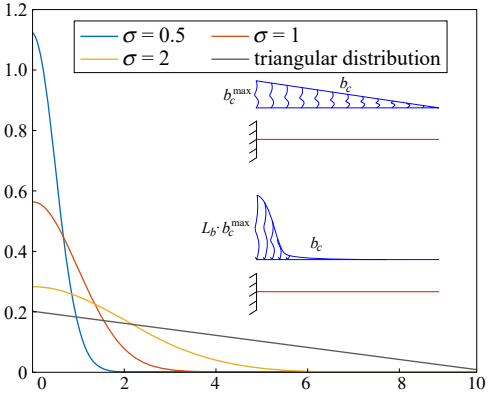

Figure 6. Three different gaussian distributions with different σ and the triangular one of b_c^{ext}.

The three different gaussian distributions (with three different maximum values at $X = 0$) and the triangular distribution are compared in Figure 6.

It is worthwhile to notice that, for the gaussian distribution, the maximum value of the externally distributed aging fluid influx pressure is $L \cdot b_{c,\max}^{\text{ext}}$, where L is the length of the beam:

$$\int_0^L b_{c,\max}^{\text{ext}} \cdot \text{triang}(X)\, dX = \int_0^L L \cdot b_{c,\max}^{\text{ext}} \cdot \text{gauss}(X)\, dX = b_{c,\max}^{\text{ext}} \cdot \frac{L}{2}, \tag{49}$$

where (i) $\text{triang}(X) = 1 - \frac{X}{L}$ represents the triangular distribution and (ii) $\text{gauss}(X) = (1/(\sigma\sqrt{2\pi}))\, e^{-(1/2)(X/\sigma)^2}$ the gaussian one. Because the considered distribution is a half gaussian curve, we have

$$\int_0^L \text{gauss}(X)\, dX \approx \tfrac{1}{2}. \tag{50}$$

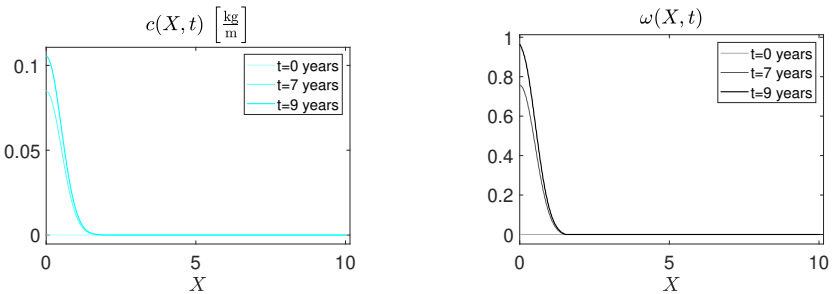

Figure 7. Left: concentration $c(X, t)$. Right: damage $\omega(X, t)$ for $\sigma = \frac{1}{2}$. The evolution in time of the kinematic quantities by a color gradient is represented. The aging evolution is represented from the lightest color to the most defined one.

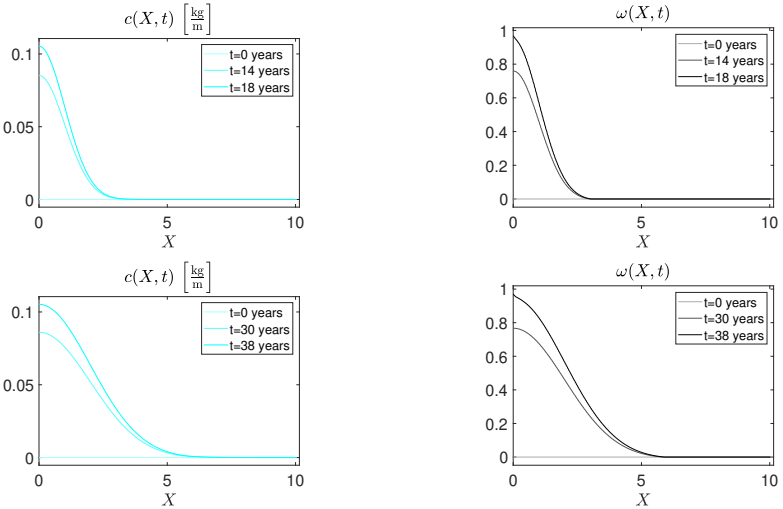

Figure 8. Top left: concentration $c(X,t)$. Top right: damage $\omega(X,t)$ for $\sigma = 1$. Bottom left: concentration $c(X,t)$. Bottom right: damage $\omega(X,t)$ for $\sigma = 2$. The evolution in time of the kinematic quantities by a color gradient is represented. The aging evolution is represented from the lightest color to the most defined one.

The results for different values of standard deviation $\sigma \in \left\{\frac{1}{2},\ 1,\ 2\right\}$ are shown in Figures 7 and 8 for the same values of other parameters given in Section 4.1. In Figure 7 the case with $\sigma = \frac{1}{2}$ is shown. In Figure 8, top, the case with $\sigma = 1$ is shown. In Figure 8, bottom, the case with $\sigma = 2$ are shown. As expected, when σ increases, we show a trend to the triangular case. These results prove that the higher the concentration of the aging fluid in one part of the beam, the lower the life time of the dam.

4.3. ***Parametric analysis:*** $\boldsymbol{K_{\text{DIF}}}$**.** In this section concentration c and damage ω are evaluated for different values of K_{DIF} such that its role can be better clarified. Four different values of K_{DIF} are considered in Figures 9 and 10 by increasing one order of magnitude compared to the previous one, as follows:

$$K_{\text{DIF}} \in \left\{10^3\ \frac{\text{m}^5}{\text{kg}\cdot\text{s}^2},\ 10^5\ \frac{\text{m}^5}{\text{kg}\cdot\text{s}^2},\ 10^7\ \frac{\text{m}^5}{\text{kg}\cdot\text{s}^2},\ 10^9\ \frac{\text{m}^5}{\text{kg}\cdot\text{s}^2}\right\}.$$

All the other parameters are equal to that given in Section 4.1.

The results in Figures 9 and 10 confirm the interpretation of K_{DIF} as a *diffusivity coefficient*. Indeed, when K_{DIF} is higher the aging fluid spreads easier into the whole body redistributing, at the same time, the damage. In particular, from Figure 10, bottom, the highest value of K_{DIF} induced the fluid to spread freely and rapidly within the body. The concentration (and the damage) distribution tend therefore

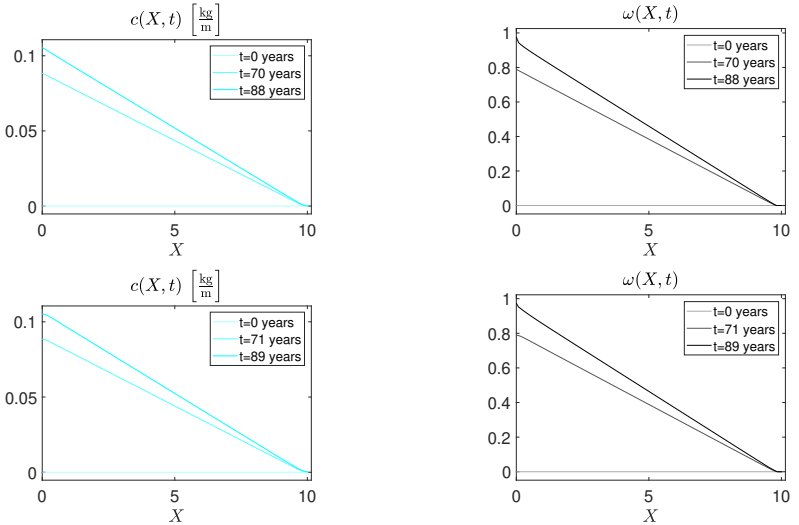

Figure 9. Top left: concentration $c(X,t)$. Top right: damage $\omega(X,t)$ for $K_{\text{DIF}} = 10^3 \frac{\text{m}^5}{\text{kg}\cdot\text{s}^2}$. Bottom left: concentration $c(X,t)$. Bottom right: damage $\omega(X,t)$ for $K_{\text{DIF}} = 10^5 \frac{\text{m}^5}{\text{kg}\cdot\text{s}^2}$. The evolution in time of the kinematic quantities by a color gradient is represented. The aging evolution is represented from the lightest color to the most defined one.

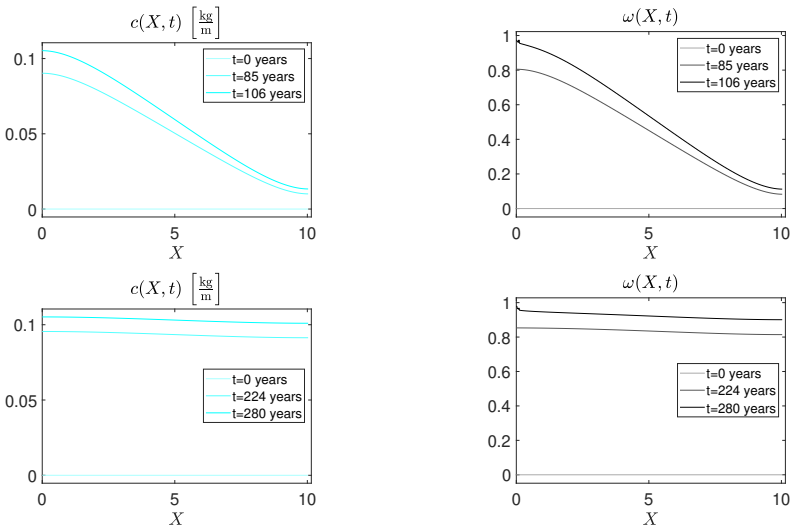

Figure 10. Top left: concentration $c(X,t)$. Top right: damage $\omega(X,t)$ for $K_{\text{DIF}} = 10^7 \frac{\text{m}^5}{\text{kg}\cdot\text{s}^2}$. Bottom left: concentration $c(X,t)$. Bottom right: damage $\omega(X,t)$ for $K_{\text{DIF}} = 10^9 \frac{\text{m}^5}{\text{kg}\cdot\text{s}^2}$. The evolution in time of the kinematic quantities by a color gradient is represented. The aging evolution is represented from the lightest color to the most defined one.

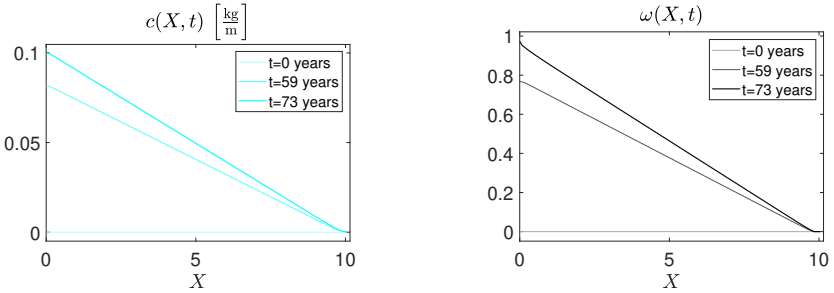

Figure 11. Concentration $c(X, t)$ (left) and damage $\omega(X, t)$ (right) for $K_{c\omega} = -9.5 \cdot 10^5 \frac{\text{J}}{\text{kg}}$. The evolution in time of the kinematic quantities by a color gradient is represented. The aging evolution is represented from the lightest color to the most defined one.

to have a rectangular shape. This means that the damage is no longer localized in a small area of the bottom of the beam and the life of the dam increases for a given b_c^{ext} distribution. This means that the failure is reached later and the life of the dam increases when the diffusivity is larger. The reason for different values of K_{DIF} may be due, for example, to the quality of the concrete. The sulfate attacks could cause an increase in porosity by allowing fluid to flow more easily within the beam. However, although the poor quality of the concrete implies higher K_{DIF}, the concentration will be more uniformly distributed and therefore the age at which damage reaches 1 is delayed.

4.4. ***Parametric analysis:*** $\boldsymbol{K_{c\omega}}$**.** We have already pointed out in (34) that the normalized undamaged energy threshold is decreased by a negative value of the concentration-damage coupling term. Thus, a parametric analysis for different values of $K_{c\omega}$ is worth doing and presented in Figure 11. The considered values of $K_{c\omega}$ are

$$K_{c\omega} \in \left\{-9.5 \frac{\text{J}}{\text{kg}}, -9 \frac{\text{J}}{\text{kg}}, -8.5 \frac{\text{J}}{\text{kg}}, -8 \frac{\text{J}}{\text{kg}}\right\} \cdot 10^5.$$

As the value of $K_{c\omega}$ varies, the behavior of the structure remains the same but the time for reaching the damage ($\omega = 1$) increases. In particular, we observe that the higher the modulus of such a coupling term, the higher the transmission of the influence of the concentration of the aging fluid on damage and the lower the life of the dam.

4.5. ***Dam's life.*** As a result of the parametric analyses in Sections 4.3 and 4.4 it is possible to analyze how the life of the dam is affected by the diffusivity characteristics and the diffusion-deformation-damage coupling. The dam's life for the triangular distribution of the external distributed aging fluid influx pressure b_c^{ext} and several values of K_{DIF} and $K_{c\omega}$ are shown in Figure 12.

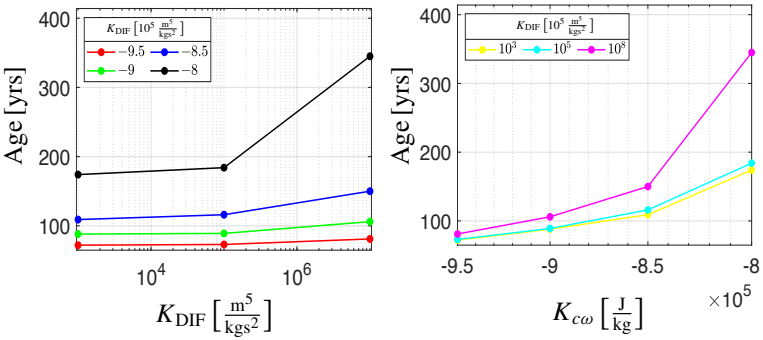

Figure 12. Left: parametric analysis for K_{DIF}. Right: parametric analysis for $K_{c\omega}$.

The results shown in Figure 12 show that if the values of K_{DIF} and $K_{c\omega}$ are higher, the dam's life increases. Figure 12, right, shows that the damage is sensitive to changes in the value of the coupling term $K_{c\omega}$.

5. Conclusions

In the above proposed formulation the evolution of the diffusion of the aging fluid, of damage and the mechanical behavior are described by the energy functional in (2) and by the hemivariational principle. Specifically, using the considered hemivariational principle, it was possible to include damage as a monotonically increasing function, that goes from 0 (nondamaged case) to 1 (complete failure), which causes the stiffnesses to fall as shown in the Section 4. By means of the term $K_{c\omega}$, which appear in the last row of the (2), the damage and the diffusion of the fluid are coupled; in this way the spreading of the fluid into the beam causes increasing of the damage and it contributes to the progress to failure. In Section 4.3 the role of the diffusivity term K_{DIF} is shown. The diffusivity represents a parameter of the material that influences the spread, and the spread rate, of the fluid within the beam. The fluid distributes along the beam and it is not localized in a small area inducing the decrease of the rate of damage and delaying the failure of the structure. Clearly, as shown in Section 4.4, the damage is affected not only by the changes of K_{DIF} but also by small changes of the coupling term $K_{c\omega}$. Increasing $K_{c\omega}$ (decrease in the value of its modulus) means the failure of the structure is delayed. The work presented here is a preliminary step which in the future will be used to develop the hemivariational method for the study of a 2-D case [51]. It will also take into account the granular micromechanics approach [3; 53; 63] so as to properly analyze the material of which the dam is composed, e.g., the concrete. Another future work will be to carry out experimental tests in order to obtain more reasonable values of the parameters K_{DIF}, $K_{c\omega}$ and K_F and, then, establish a more realistic distribution

of b_c^{ext}. It is worth noticing that the study of the diffusion of an aging agent within a human-made construct is not limited to the case of dams. The formulation can have several different fields of application, for example, all those problems that involve diffusion in porous material [35]. It could help, for example, in the monitoring and safeguarding of the objects of artistic-cultural heritage and having, for the future structures, more careful design that tends to protect the artifacts from the diffusion of slag [38; 62] or pollutants that are abundant nowadays in our cities.

References

[1] B. E. Abali, A. Klunker, E. Barchiesi, and L. Placidi, "A novel phase-field approach to brittle damage mechanics of gradient metamaterials combining action formalism and history variable", *ZAMM Z. Angew. Math. Mech.* **101**:9 (2021), art. id. e202000289.

[2] M. Alexander and H. Beushausen, "Durability, service life prediction, and modelling for reinforced concrete structures — review and critique", *Cement and Concrete Research* **122** (2019), 17–29.

[3] M. D. Angelo, L. Placidi, N. Nejadsadeghi, and A. Misra, "Non-standard Timoshenko beam model for chiral metamaterial: identification of stiffness parameters", *Mechanics Research Communications* **103** (2020), art. id. 103462.

[4] I. T. Ardic, M. E. Yildizdag, and A. Ergin, "An FE-BE method for the hydroelastic vibration analysis of plates and shells partially in contact with fluid", pp. 267–300 in *Developments and novel approaches in nonlinear solid body mechanics*, edited by B. E. Abali and I. Giorgio, Adv. Struct. Mater. **130**, Springer, 2020.

[5] N. Auffray, F. dell'Isola, V. A. Eremeyev, A. Madeo, and G. Rosi, "Analytical continuum mechanics *à la* Hamilton–Piola least action principle for second gradient continua and capillary fluids", *Math. Mech. Solids* **20**:4 (2015), 375–417.

[6] E. Barchiesi and N. Hamila, "Maximum mechano-damage power release-based phase-field modeling of mass diffusion in damaging deformable solids", *Z. Angew. Math. Phys.* **73**:1 (2022), art. id. 35.

[7] J. A. Bather, "A diffusion model for the control of a dam", *J. Appl. Probability* **5** (1968), 55–71.

[8] Z. P. Bažant and S. T. Wu, "Dirichlet series creep function for aging concrete", *Journal of the Engineering Mechanics Division* **99**:2 (1973), 367–387.

[9] Z. P. Bažant and S. T. Wu, "Rate-type creep law of aging concrete based on maxwell chain", *Matériaux et Constructions* **7**:1 (1974), 45–60.

[10] M. Bîrsan, H. Altenbach, T. Sadowski, V. Eremeyev, and D. Pietras, "Deformation analysis of functionally graded beams by the direct approach", *Composites Part B: Engineering* **43**:3 (2012), 1315–1328.

[11] L. Capacci, F. Biondini, and A. Titi, "Lifetime seismic resilience of aging bridges and road networks", *Structure and Infrastructure Engineering* **16**:2 (2019), 266–286.

[12] J. Pla i Carrera, "Joseph-Louis Lagrange: in memoriam", *Butl. Soc. Catalana Mat.* **29**:2 (2014), 135–165.

[13] A. Cazzani, M. Malagù, and E. Turco, "Isogeometric analysis of plane-curved beams", *Math. Mech. Solids* **21**:5 (2016), 562–577.

[14] N. Cefis and C. Comi, "Damage modelling in concrete subject to sulfate attack", *Frattura ed Integrità Strutturale* **8**:29 (2014), 222–229.

[15] N. Cefis and C. Comi, "Chemo-mechanical modelling of the external sulfate attack in concrete", *Cement and Concrete Research* **93** (2017), 57–70.

[16] X. Chai, Q. Luo, and J. Zhu, "A simple and practical pulp kappa test method for process control in pulp production", *Process Control and Quality* **11**:5 (2000), 407–417.

[17] B. Chiaia, V. De Biagi, and L. Placidi, "A damaged non-homogeneous Timoshenko beam model for a dam subjected to aging effects", *Math. Mech. Solids* **26**:5 (2021), 694–707.

[18] A. Ciallella, D. Pasquali, M. Gołaszewski, F. D'Annibale, and I. Giorgio, "A rate-independent internal friction to describe the hysteretic behavior of pantographic structures under cyclic loads", *Mechanics Research Communications* **116** (2021), art. id. 103761.

[19] A. Ciallella, D. Scerrato, M. Spagnuolo, and I. Giorgio, "A continuum model based on Rayleigh dissipation functions to describe a Coulomb-type constitutive law for internal friction in woven fabrics", *Z. Angew. Math. Phys.* **73**:5 (2022), art. id. 209.

[20] M. Colombo and C. Comi, "Hydro-thermo-mechanical analysis of an existing gravity dam undergoing alkali-silica reaction", *Infrastructures* **4**:3 (2019), art. id. 55.

[21] C. Comi, R. Fedele, and U. Perego, "A chemo-thermo-damage model for the analysis of concrete dams affected by alkali-silica reaction", *Mechanics of Materials* **41**:3 (2009), 210–230.

[22] M. Cuomo, "Continuum damage model for strain gradient materials with applications to 1D examples", *Contin. Mech. Thermodyn.* **31**:4 (2019), 969–987.

[23] M. Cuomo and A. Nicolosi, "A poroplastic model for hygro-chemo-mechanical damage of concrete", pp. 533–542 in *Computational Modelling of Concrete Structures* (Mayrhofen, Austria, 2006).

[24] F. D'Annibale, M. Ferretti, and A. Luongo, "Shear-shear-torsional homogenous beam models for nonlinear periodic beam-like structures", *Engineering Structures* **184** (2019), 115–133.

[25] A. Della Corte, F. dell'Isola, R. Esposito, and M. Pulvirenti, "Equilibria of a clamped Euler beam (*elastica*) with distributed load: large deformations", *Math. Models Methods Appl. Sci.* **27**:8 (2017), 1391–1421.

[26] A. Della Corte, A. Battista, F. dell'Isola, and P. Seppecher, "Large deformations of Timoshenko and Euler beams under distributed load", *Z. Angew. Math. Phys.* **70**:2 (2019), art. id. 52.

[27] F. dell'Isola and L. Placidi, "Variational principles are a powerful tool also for formulating field theories", pp. 1–15 in *Variational models and methods in solid and fluid mechanics*, edited by F. dell'Isola and S. Gavrilyuk, CISM Courses and Lect. **535**, Springer, 2011.

[28] F. Dell'Isola and C. Woźniak, "On phase transition layers in certain micro-damaged two-phase solids", *International Journal of Fracture* **83**:2 (1997), 175–189.

[29] F. dell'Isola, A. Della Corte, and I. Giorgio, "Higher-gradient continua: the legacy of Piola, Mindlin, Sedov and Toupin and some future research perspectives", *Math. Mech. Solids* **22**:4 (2017), 852–872.

[30] F. dell'Isola, I. A. Volkov, L. A. Igumnov, S. R. Eugster, S. Y. Litvinchuk, D. A. Kazakov, V. A. Gorohov, and B. E. Abali, "Estimating fatigue related damage in alloys under block-type non-symmetrical low-cycle loading", pp. 81–92 in *New achievements in continuum mechanics and thermodynamics*, edited by B. E. Abali et al., Adv. Struct. Mater. **108**, Springer, 2019.

[31] V. A. Eremeyev, F. S. Alzahrani, A. Cazzani, F. dell'Isola, T. Hayat, E. Turco, and V. Konopińska-Zmysłowska, "On existence and uniqueness of weak solutions for linear pantographic beam lattices models", *Contin. Mech. Thermodyn.* **31**:6 (2019), 1843–1861.

[32] L. Eulerus, *Methodus inveniendi lineas curvas maximi minimive proprietate gaudentes sive solutio problematis isoperimetrici latissimo sensu accepti*, Springer, Basel, 1952.

[33] I. Giorgio, "A variational formulation for one-dimensional linear thermoviscoelasticity", *Math. Mech. Complex Syst.* **9**:4 (2021), 397–412.

[34] I. Giorgio and D. Scerrato, "Multi-scale concrete model with rate-dependent internal friction", *European Journal of Environmental and Civil Engineering* **21**:7-8 (2016), 821–839.

[35] I. Giorgio, F. dell'Isola, U. Andreaus, F. Alzahrani, T. Hayat, and T. Lekszycki, "On mechanically driven biological stimulus for bone remodeling as a diffusive phenomenon", *Biomechanics and Modeling in Mechanobiology* **18**:6 (2019), 1639–1663.

[36] L. Greco, A. Scrofani, and M. Cuomo, "A non-linear symmetric G^1-conforming Bézier finite element formulation for the analysis of Kirchhoff beam assemblies", *Comput. Methods Appl. Mech. Engrg.* **387** (2021), art. id. 114176.

[37] L. Greco, M. Cuomo, D. Castello, and A. Scrofani, "An updated Lagrangian Bézier finite element formulation for the analysis of slender beams", *Math. Mech. Solids* **27**:10 (2022), 2110–2138.

[38] C. Guo, B. Sun, D. Hu, F. Wang, M. Shi, and X. Li, "A field experimental study on the diffusion behavior of expanding polymer grouting material in soil", *Soil Mechanics and Foundation Engineering* **56**:3 (2019), 171–177.

[39] C. C. Habeger, D. W. Coffin, and B. Hojjatie, "Influence of humidity cycling parameters on the moisture-accelerated creep of polymeric fibers", *Journal of Polymer Science Part B*: *Polymer Physics* **39**:17 (2001), 2048–2062.

[40] W. Hong, X. Zhao, J. Zhou, and Z. Suo, "A theory of coupled diffusion and large deformation in polymeric gels", *Journal of the Mechanics and Physics of Solids* **56**:5 (2008), 1779–1793.

[41] T. Hromadka, C. Berenbrock, J. Freckleton, and G. Guymon, "A two-dimensional dam-break flood plain model", *Advances in Water Resources* **8**:1 (1985), 7–14.

[42] I. H. Kim, H. Jeon, S. C. Baek, W. H. Hong, and H. J. Jung, "Application of crack identification techniques for an aging concrete bridge inspection using an unmanned aerial vehicle", *Sensors* (*Basel*) **18**:6 (2018), 1–14.

[43] J.-L. Lagrange, *Mécanique analytique, II*, Cambridge Univ. Press, 1788.

[44] M. Malikan and V. A. Eremeyev, "A new hyperbolic-polynomial higher-order elasticity theory for mechanics of thick FGM beams with imperfection in the material composition", *Composite Structures* **249** (2020), arti. id. 112486.

[45] A. Misra, L. Placidi, and E. Turco, "Variational methods for discrete models of granular materials", pp. 2621–2634 in *Encyclopedia of Continuum Mechanics*, Springer, 2020.

[46] T. H. A. Nguyen and J. Niiranen, "A second strain gradient damage model with a numerical implementation for quasi-brittle materials with micro-architectures", *Math. Mech. Solids* **25**:3 (2020), 515–546.

[47] R. P. L. Nijssen, "Fatigue life prediction and strength degradation of wind turbine rotor blade composites", 2007, available at https://energy.sandia.gov/wp-content/gallery/uploads/SAND-2006-7810p.pdf.

[48] M. Paradiso, S. Sessa, N. Vaiana, F. Marmo, and L. Rosati, "Shear properties of isotropic and homogeneous beam-like solids having arbitrary cross sections", *International Journal of Solids and Structures* **216** (2021), 231–249.

[49] L. Placidi, "A variational approach for a nonlinear 1-dimensional second gradient continuum damage model", *Contin. Mech. Thermodyn.* **27**:4-5 (2015), 623–638.

[50] L. Placidi, "A variational approach for a nonlinear one-dimensional damage-elasto-plastic second-gradient continuum model", *Contin. Mech. Thermodyn.* **28**:1-2 (2016), 119–137.

[51] L. Placidi, A. Misra, and E. Barchiesi, "Two-dimensional strain gradient damage modeling: a variational approach", *Z. Angew. Math. Phys.* **69**:3 (2018), art. id. 56.

[52] L. Placidi, E. Barchiesi, A. Misra, and U. Andreaus, "Variational methods in continuum damage and fracture mechanics", pp. 2634–2643 in *Encyclopedia of Continuum Mechanics*, Springer, 2020.

[53] L. Placidi, E. Barchiesi, A. Misra, and D. Timofeev, "Micromechanics-based elasto-plastic-damage energy formulation for strain gradient solids with granular microstructure", *Contin. Mech. Thermodyn.* **33**:5 (2021), 2213–2241.

[54] L. Placidi, E. Barchiesi, F. dell'Isola, V. Maksimov, A. Misra, N. Rezaei, A. Scrofani, and D. Timofeev, "On a hemi-variational formulation for a 2D elasto-plastic-damage strain gradient solid with granular microstructure", *Math. Eng.* **5**:1 (2023), art. id. 021.

[55] K. R. Rajagopal, "Diffusion through polymeric solids undergoing large deformations", *Materials Science and Technology* **19**:9 (2003), 1175–1180.

[56] K. Rajagopal, A. Srinivasa, and A. Wineman, "On the shear and bending of a degrading polymer beam", *International Journal of Plasticity* **23**:9 (2007), 1618–1636.

[57] I. Shames and J. Pitarresi, *Introduction to solid mechanics*, Prentice Hall, 2000.

[58] H.-W. Song, S.-J. Kwon, K.-J. Byun, and C.-K. Park, "Predicting carbonation in early-aged cracked concrete", *Cement and Concrete Research* **36**:5 (2006), 979–989.

[59] M. Spagnuolo and U. Andreaus, "A targeted review on large deformations of planar elastic beams: extensibility, distributed loads, buckling and post-buckling", *Math. Mech. Solids* **24**:1 (2019), 258–280.

[60] M. Spagnuolo, K. Barcz, A. Pfaff, F. dell'Isola, and P. Franciosi, "Qualitative pivot damage analysis in aluminum printed pantographic sheets: numerics and experiments", *Mechanics Research Communications* **83** (2017), 47–52.

[61] F. Stochino, A. Cazzani, G. F. Giaccu, and E. Turco, "Dynamics of strongly curved concrete beams by isogeometric finite elements", pp. 231–247 in *Lecture Notes in Civil Engineering*, Springer, 2018.

[62] M. D. Thomas and P. B. Bamforth, "Modelling chloride diffusion in concrete", *Cement and Concrete Research* **29**:4 (1999), 487–495.

[63] D. Timofeev, E. Barchiesi, A. Misra, and L. Placidi, "Hemivariational continuum approach for granular solids with damage-induced anisotropy evolution", *Math. Mech. Solids* **26**:5 (2021), 738–770.

[64] N. Vaiana, R. Capuano, S. Sessa, F. Marmo, and L. Rosati, "Nonlinear dynamic analysis of seismically base-isolated structures by a novel opensees hysteretic material model", *Applied Sciences* **11**:3 (2021), 900.

[65] I. Vlahinić, J. J. Thomas, H. M. Jennings, and J. E. Andrade, "Transient creep effects and the lubricating power of water in materials ranging from paper to concrete and kevlar", *J. Mech. Phys. Solids* **60**:7 (2012), 1350–1362.

[66] J. Voges, F. Duvigneau, and D. Juhre, "On the deformation dependency of the diffusion flux in solids at large deformations", *Contin. Mech. Thermodyn.* **34**:3 (2022), 829–839.

[67] J. Z. Wang, D. A. Dillard, and F. A. Kamke, "Transient moisture effects in materials", *Journal of Materials Science* **26**:19 (1991), 5113–5126.

[68] S. Wilcot John, R. Lindsay, R. T. Newman, and A. D. Joseph, "Modelling and measurement of radon diffusion through soil for application on mine tailings dams", *Arab J. Nucl. Sci. Appl.* **38** (2005), 279–287.

[69] M. E. Yildizdag, I. T. Ardic, and A. Ergin, "An isogeometric FE-BE method to investigate fluid–structure interaction effects for an elastic cylindrical shell vibrating near a free surface", *Ocean Engineering* **251** (2022), art. id. 111065.

Received 16 Nov 2022. Revised 19 Dec 2022. Accepted 10 Jan 2023.

ANGELO SCROFANI: angelo.scrofani@graduate.univaq.it
Dipartimento di Ingegneria e Scienze dell'Informazione Matematica, Università degli Studi dell'Aquila, L'Aquila, Italy

EMILIO BARCHIESI: ebarchiesi@uniss.it
Dipartimento di Architettura, Università degli Studi di Sassari, Alghero, Italy

BERNARDINO CHIAIA: bernardino.chiaia@polito.it
Dipartimento di Ingegneria Strutturale, Edile e Geotecnica, Politecnico di Torino, Torino, Italy

ANIL MISRA: amisra@ku.edu
Civil, Environmental and Architectural Engineering Department, University of Kansas, Lawrence, KS, United States

LUCA PLACIDI: luca.placidi@uninettunouniversity.net
Engineering Faculty, International Telematic University Uninettuno, Roma, Italy

MATHEMATICS AND MECHANICS OF COMPLEX SYSTEMS

msp.org/memocs

MEMOCS is a journal of the International Research Center for the Mathematics and Mechanics of Complex Systems at the Università dell'Aquila, Italy.

See inside back cover or msp.org/memocs for submission instructions.

The subscription price for 2023 is US $195/year for the electronic version, and $255/year (+$25, if shipping outside the US) for print and electronic. Subscriptions, requests for back issues and changes of subscriber address should be sent to MSP.

Mathematics and Mechanics of Complex Systems (ISSN 2325-3444 electronic, 2326-7186 printed) at Mathematical Sciences Publishers, 798 Evans Hall #3840, c/o University of California, Berkeley, CA 94720-3840 is published continuously online.

MEMOCS peer review and production are managed by EditFlow® from MSP.

PUBLISHED BY
mathematical sciences publishers
nonprofit scientific publishing
http://msp.org/

Mathematics and Mechanics of Complex Systems
vol. 11 no. 2 2023

MEMOCS is a journal of the International Research Center for the Mathematics and Mechanics of Complex Systems at the Università dell'Aquila, Italy.